



RESEARCH ARTICLE

10.1029/2023JG007705

Key Points:

- Fecal pellet-like dinoflagellates (FLDs) were observed among drifting sediment trap samples in the East Antarctic ice zone
- FLD cells were identified as *Gyrodinium rubrum* and *Gyrodinium heterogrammum*
- FLDs determined as potential players for carbon export that were overlooked because of their appearance

Supporting Information:

Supporting Information may be found in the online version of this article.

Correspondence to:

R. Matsuda,
ryomatsuda@soka.gr.jp

Citation:

Matsuda, R., Makabe, R., Sano, M., Takao, S., Moteki, M., & Kurosawa, N. (2023). Fecal pellet-like *Gyrodinium* species in sinking particles: Newly found potential contributors for carbon export in the Antarctic seasonal ice zone. *Journal of Geophysical Research: Biogeosciences*, 128, e2023JG007705. <https://doi.org/10.1029/2023JG007705>

Received 12 JUL 2023

Accepted 14 SEP 2023





Author Contributions:

Conceptualization: R. Matsuda, R. Makabe, N. Kurosawa
Data curation: R. Matsuda
Formal analysis: R. Matsuda
Funding acquisition: R. Matsuda, R. Makabe, M. Moteki
Investigation: R. Matsuda, R. Makabe, M. Sano, S. Takao
Project Administration: R. Makabe, N. Kurosawa
Resources: R. Makabe, N. Kurosawa
Supervision: R. Makabe, N. Kurosawa
Visualization: R. Matsuda
Writing – original draft: R. Matsuda

© 2023. The Authors.

This is an open access article under the terms of the [Creative Commons Attribution License](https://creativecommons.org/licenses/by/4.0/), which permits use, distribution and reproduction in any medium, provided the original work is properly cited.

Fecal Pellet-Like *Gyrodinium* Species in Sinking Particles: Newly Found Potential Contributors for Carbon Export in the Antarctic Seasonal Ice Zone

R. Matsuda¹ , R. Makabe^{2,3,4}, M. Sano^{2,5} , S. Takao⁶ , M. Moteki^{2,3}, and N. Kurosawa¹ 

¹Department of Environmental Engineering for Symbiosis, Graduate School of Science and Engineering, Soka University, Tokyo, Japan, ²National Institute of Polar Research, Tokyo, Japan, ³Department of Ocean Sciences, Tokyo University of Marine Science and Technology, Tokyo, Japan, ⁴Department of Polar Science, The Graduate University for Advanced Studies (SOKENDAI), Tokyo, Japan, ⁵Now at Atmosphere and Ocean Research Institute, The University of Tokyo, Kashiwa, Japan, ⁶National Institute for Environmental Studies, Ibaraki, Japan

Abstract Fecal pellets (FPs) are generated by various species and have gained attention as contributors to the biological carbon pump. Metazoans and protozoans are known as FP and minipellet-producers, respectively. Herein, we discovered fecal pellet-like dinoflagellates (FLDs) in the seasonal sea ice zone in the Southern Ocean. The size and form of these FLDs were similar to those of zooplankton oval FPs. However, due to their appearance, they have been misclassified as FPs rather than dinoflagellates, leading to potential oversight of their role in the carbon cycle. Thus, we aimed to identify FLD cells at the species level and examine the impact of FLDs on flux estimation of particulate organic carbon (POC). Our findings are as follows: first, FLD cells were identified as *Gyrodinium rubrum* and *Gyrodinium heterogrammum* through 18S rRNA gene sequencing. Second, FLDs can potentially excrete larger FPs than minipellets. Third, the sinking rate of FLDs is higher than that of other protozoa and dinoflagellate cysts. Finally, a maximum of 12 mgC m⁻² day⁻¹ of the POC flux can be attributed to FLDs (representing 32% of POC flux). These results suggest that FLDs are important drivers not only for the microbial loop but also for the biological carbon pump. In future projections of carbon sequestration, the contribution of metazoans to carbon export must be considered, but not that of FLDs. Their unknown physiological and ecological characteristics, especially including the responses to climate changes, must be urgently investigated for future projections of carbon sequestration in the Southern Ocean.

Plain Language Summary Zooplankton feed on phytoplankton cells and excrete fecal pellets (FPs). FPs have gained attention as carbon carriers from the surface to the deep ocean because of their high carbon contents and sinking rate. Previous studies have sampled FPs using sediment traps and estimated carbon fluxes through microscopic observations to better understand the ocean carbon cycle. Here, we report the discovery of a dinoflagellate that closely resembles FP and was captured using a drifting sediment trap. This dinoflagellate has been named “fecal-pellet-like dinoflagellate (FLD).” It is believed that FLD cells have been misclassified as FPs given their appearance. Our findings indicated that a maximum of 12 mgC m⁻² day⁻¹ (representing 32% of the particulate organic carbon flux at 50 m depths during the summer productive season) may be attributed to FLD carbon flux. This result suggests that FLD cells serve as potential contributors for carbon export, contrary to the knowledge that heterotrophic dinoflagellates had been known as one of the dominant microbial loop components. Studies on FLDs are essential to understand the Southern Ocean carbon cycle.

1. Introduction

The biological carbon pump is an essential process for transferring CO₂ from the atmosphere to the deep ocean (Honjo et al., 2014; Turner, 2015). Phytoplankton cells absorb and store carbon through photosynthesis, and this fixed carbon sinks as particulate organic carbon (POC) in various forms, including zooplankton fecal pellets (FPs), aggregates (marine snow), and zooplankton carcasses. In contrast, the grazing activity of protozoans such as ciliates and heterotrophic dinoflagellates converts large POCs to smaller particles including dissolved organic carbon (DOC). Therefore, heterotrophic protozoa are known as components of the microbial loop (Steinberg & Landry, 2017). POC and DOC that are not remineralized can be sequestered in the deep ocean or as sediments on the seafloor. Carbon is considered to be sequestered on climatically relevant timescales when it is stored away from the atmosphere for 100 years or more (IPCC, 2007). Therefore, investigating the complex processes of the

Writing – review & editing: R. Matsuda, R. Makabe, M. Sano, S. Takao, M. Moteki, N. Kurosawa

biological carbon pump is crucial for a better understanding of the global carbon cycle and climate (Passow & Carlson, 2012; Turner, 2015).

The contribution of recognizable zooplankton FPs to the total POC export varies widely, ranging from <1% to almost 100% (Steinberg & Landry, 2017). Zooplankton FPs play a significant role in carbon export to deeper waters but with highly variable contributions due to degradation, fragmentation, and repackaging processes (Steinberg & Landry, 2017; Turner, 2015). Different types of FPs are produced by different organisms, such as cylindrical FPs by euphausiids, salps, and large copepods (Bathmann et al., 1990; Beaumont et al., 2001); ellipsoidal FPs by larvaceans such as chaetognaths and heteropods (Dilling & Alldredge, 1993; Taguchi & Saino, 1998; Wilson et al., 2008); oval pellets by pteropods, chaetognaths, and small copepods (Gonzalez, 1992; Manno et al., 2015); and minipellets (less than 60 μm in diameter) by zooplankton nauplii and heterotrophic protozoa (Buck & Newton, 1995; Gonzalez, 1992; Gowing & Silver, 1985). These FPs have different roles in carbon export because of their varying sizes, sinking rates, and fluxes.

Heterotrophic dinoflagellates, ciliates, and radiolarians have been known to produce minipellets (Beaumont et al., 2002; Gonzalez, 1992; Gowing & Silver, 1985). However, their contribution to carbon export was thought to be limited. Minipellets generated by *Gyrodinium* sp. are considered ineffective carbon carriers in the deep sea due to their low sinking rates, making them prone to remineralization in the epipelagic region (Saito et al., 2006). Moreover, heterotrophic dinoflagellates such as *Gyrodinium dominans*, *G. spirale*, and *Protoberidinium* spp. can feed on FPs produced by copepods (Poulsen & Iversen, 2008; Poulsen et al., 2011). Ciliates and dinoflagellates can degrade large copepod FPs (Svensen et al., 2012). Therefore, heterotrophic protozoa, including ciliates and heterotrophic dinoflagellates, are considered consumers of POC and DOC in the microbial loop, contributing to the attenuation of carbon flux.

Heterotrophic dinoflagellates play an important role in trophic links between phytoplankton or prokaryotes and higher-order consumers. A phagotrophic athecate dinoflagellate was observed in the floating sea ice and adjacent water column along the coast of the Weddell Sea (Buck et al., 1990). This dinoflagellate was identified as a potential minipellet producer based on the size and similarity between the food vacuoles of the dinoflagellate and the contents of minipellets. It was speculated that the release of the dinoflagellates and their FPs might significantly contribute to the POC available to higher-order consumers.

In our field observation, a time-series drifting sediment trap was deployed in the seasonal ice zone of the Southern Ocean. The drifting sediment trap captured a dinoflagellate resembling a zooplankton FP (more details are provided in the Results and Discussion). This dinoflagellate was named “fecal pellet-like dinoflagellate (FLD)” based on its appearance. The size of heterotrophic dinoflagellate cells can change due to grazing activity and FP production (Buck et al., 2005; Saito et al., 2006). However, whether dinoflagellates increase in size through grazing activity and sink themselves has not yet been reported. Owing to their appearance, these FLDs might have been misclassified as FPs rather than dinoflagellates, which could have led to an overestimation of FP carbon flux. Additionally, the role of FLD cells in the food chain and carbon cycle may have been overlooked. Thus, in this study, we aimed to identify FLD cells at the species level and examine their impact on the estimation of FP carbon flux. Here, we describe the identification of FLD cells at the species level and provide information on their FPs, potential sinking rate, and potential flux.

2. Materials and Methods

2.1. Study Site and Sampling

Field observations were conducted three times in the seasonal ice zone of the Indian sector of the Southern Ocean. In the first observation, a drifting sediment trap was deployed in 10 December 2016 during the icebreaker *Shirase* cruise of the 58th Japanese Antarctic Research Expedition (JARE). It was recovered in 3 January 2017 during the Antarctic cruises of the training vessel (TV) *Umitaka-maru* of the Tokyo University of Marine Science and Technology. In the second observation, drifting sediment traps were deployed and recovered from 14 January 2018 to 19 January 2018 during the Antarctic cruises of the TV *Umitaka-maru*. In the third observation, drifting sediment traps were deployed in 10 December 2019 and recovered in 16 February 2020 during the icebreaker *Shirase* cruise of the 61st JARE. A drifter array, equipped with various sensors and time-series sediment traps (SMC7S-500, Nichiyu Giken Kogyo, Japan), was also deployed (Figures S1 and S2 in Supporting Information S1). Sampling cups (500 mL) were filled with filtered seawater supplemented with NaCl (final concentration, 5.0%)

and neutral Lugol's solution (final concentration, 10% or 20%, depending on the sampling duration). During the 2016–2017 and 2019–2020 observations, temperature, salinity, oxygen concentration, and in situ chlorophyll fluorescence were measured at the deployment and retrieval sites using a conductivity-temperature-depth (CTD) device (SBE-9plus; Sea-Bird Electronics, Bellevue, WA, USA). During the observation in January 2018, these parameters were measured near the drifter using a CTD system comprising a CTD SBE9plus and a 24-position carousel water sampler provided by Sea-Bird Electronics, Inc. Niskin bottles (8 L) were mounted on the frame and used for sampling water.

2.2. Pre-Treatment of the Sediment Trap Samples

Prior to the analysis, the metazoans with sizes greater than 1.5 mm were removed as swimming zooplanktons from the sinking particle samples by using a stereomicroscope (Olympus SZX7, Olympus Inc., Japan). Notably, sediment traps also collect actively swimming zooplankton, but these were not included in the analysis as sinking particles (Michaels et al., 1990; Yokoi et al., 2018). After removing the swimming zooplankton, the sinking particle samples were split using a Motoda plankton sample splitter (Motoda, 1959). Each divided sample was used for morphological observation, high-throughput DNA sequencing, flux estimation, and POC analysis.

2.3. Morphological Analyses Using 4',6-Diamidino-2-Phenylindole Stain

The FLD cells were isolated from the divided sample, and sodium thiosulfate was added to the FLD cells to remove Lugol's iodine solution. The treated samples were stained with 4',6-diamidino-2-phenylindole (DAPI) at a final concentration of $1 \mu\text{g mL}^{-1}$. The samples were observed using a differential interference-contrast microscope (Eclipse 80i, Nikon Co., Japan) with a UV-2a filter (excitation, 330–380 nm; barrier filter, 420 nm; Nikon Co.).

2.4. Morphological Analyses Using Electron Microscopy

Microscopic observations were conducted using electron microscopy. FLD cells fixed using 10% Lugol's solution were obtained and rinsed thrice with distilled water to remove salts from the samples. Each rinsed cell was placed in a clean Petri dish containing 0.001% Triton X-100 and mixed 10 times through repeated pipetting to remove any deposits, such as detritus, for better observation. Subsequently, each cell was attached to a carbon stub using double-sided tape. The cell on the carbon stub was rapidly frozen by applying a small copper column block (Cooling Unit FDC10, SUN Technologies, Japan) at -100°C . The cells were dehydrated using a freeze dryer (FD-6510, SUN Technologies). With the cell in place, the carbon stub was sputter-coated with osmium for 5 s using an osmium coater (HPC-1SW, Vacuum Device Co. Ltd., Japan). The cell morphology was examined using a field-emission scanning electron microscope (JSM-7500F, JEOL, Japan).

2.5. *Gyrodinium*-Specific PCR Primer Design

A *Gyrodinium*-specific Polymerase Chain Reaction (PCR) primer set was designed for the 18S rRNA gene using the published sequences of the 18S rRNA genes of 12 species within this genus (Table S1 in Supporting Information S1) and the NCBI primer basic local alignment search tool (BLAST) program (Ye et al., 2012). The specificity of the primer set was analyzed using the Silva-TestPrime program (Klindworth et al., 2013).

2.6. PCR Amplification and Sanger Sequencing

Twenty-eight FLD cells (18 cells at 60 m depth and 10 cells at 150 m depth) were sorted from the sinking particles sampled in January 2019. The nuclei on the surface of the cells were separated from the cells using a needle and a stereomicroscope (Olympus SZX7, Olympus Inc.). The nuclear DNA of each cell was homogenized in 5% Chelex® 100 using a hand-held pestle homogenizer (Nagai et al., 2012). Subsequently, the solutions were incubated at 100°C for 20 min (Peng et al., 2013). The partial 18S rRNA genes were amplified from the extracted DNA using the E562F/E1642R primer set (Wang et al., 2014) (Table S2 in Supporting Information S1) and the EmeraldAmp MAX PCR Master Mix (Takara Bio) under the following conditions: 94°C for 3 min; 35 cycles of 94°C for 30 s, 67°C for 30 s, and 72°C for 70 s; and a final extension at 72°C for 5 min.

In another set of samples collected between December 2019 and January 2020, 66 FLD cells (53 cells at 60 m depth and 13 cells at 150 m depth) were sorted from the sinking particles. The total DNA of each cell was extracted using 100 μL of lysis buffer (10 mM Tris-HCl, pH 8.0, 0.5% Polyoxyethylene (20) Sorbitan Monolaurate, 50 mM KCl, and 20 mg mL^{-1} proteinase K) under the following conditions: 65°C for 15 min and 95°C for 15 min. The partial 18S rRNA genes were amplified from the extracted DNA using the *Gyrodinium*-specific primer set (Table S2 in Supporting Information S1) and the Emerald Amp MAX PCR Master Mix (Takara Bio) under the following conditions: 94°C for 3 min; 30 cycles of 94°C for 30 s, 56°C for 30 s, and 72°C for 2 min; and a final extension at 72°C for 3 min. The PCR product was purified using the Agencourt AMPure XP PCR clean-up kit (Beckman Coulter, California, USA), according to the manufacturer's instructions. Each PCR product was sequenced by Eurofins Genomics (Eurofins, Japan) using Sanger sequencing technology.

2.7. Homology and Phylogenetic Tree Analyses

Phylogenetic analyses of the 18S rRNA gene sequences were performed using the MEGA7 software (Kumar et al., 2016). A homology search was conducted using BLAST. A neighbor-joining tree, including bootstrap probabilities (1,000 replicates), was constructed using the published sequences of *Gyrodinium* species from the GenBank database and MEGA7. Multiple sequence alignment was carried out using the MUSCLE program, as implemented in MEGA7 (Edgar, 2004).

2.8. Size, Sinking Rate, and Flux Estimations

The cylindrical and ellipsoidal FPs, as well as FLD cells, were counted using a light microscope (Olympus IX71, Olympus Inc., Japan) based on morphological features such as the nuclei, protrusions, and grid-like patterns on the cell surface. The diameter and length of the FPs and FLD cells were measured using open-source image analysis software (Karasunpo, Katayama Hirofumi Mz, Japan). The sinking rates were obtained using the equation based on Stokes' law (Komar et al., 1981):

$$V = 0.079 \times \frac{1}{\mu} \times (\rho_{\text{FLD}} - \rho_{\text{SW}}) \times g \times d^2 \left(\frac{l}{d}\right)^{-1.664} \quad (1)$$

where μ is the kinetic viscosity of seawater (0.0189 g $\text{cm}^{-1} \text{s}^{-1}$ that was measured value at 10 m and deep-chlorophyll maximum along 80°E transect; Seuront et al., 2010); ρ_{FLD} is the density of the FLD (three reported density values, including 1.09 g cm^{-3} for living *Gyrodinium* cells, 1.14 g cm^{-3} for *Gyrodinium* cysts, and 1.19 g cm^{-3} for spherical FPs, were used as the ρ_{FLD}) (Anderson et al., 1985; Atkinson et al., 2012; Kamykowski et al., 1992); ρ_{SW} is the density of seawater (1.028 g cm^{-3} that was maximum value at 60 and 150 m when drifting sediment traps were deployed and recovered); l and d are the FP length (μm) and diameter (μm), respectively; and g is the acceleration due to gravity (981 cm s^{-2}).

Fluxes were calculated using the following equation:

$$F = N \times \frac{1}{0.019 \text{ m}^2} \times \frac{1}{d} \quad (2)$$

where F (#FP or cells $\text{m}^{-2} \text{day}^{-1}$) is the flux of the ellipsoidal FPs or FLD cells, N is the number of individuals or cells in each sample, 0.019 m^2 is the trap mouth area, and d is the interval space between each sample (2016: 4 days, 2019: 1 day, 2020: 6 days).

The FP carbon content was calculated based on a conversion factor of 0.038, 0.03, and 0.02 mg C mm^{-3} for cylindrical FPs and 0.041, 0.038, and 0.034 mg C mm^{-3} for oval or ellipsoidal FPs (Gleiber et al., 2012; Manno et al., 2015; Rembauville et al., 2015). The FLD carbon content was calculated using various conversion factors for living dinoflagellates (Menden-Deuer & Lessard, 2000), *G. dominans* cells (Archer et al., 1996; Nakamura et al., 1992), and FP (Manno et al., 2015). Carbon fluxes were calculated using the following equation:

$$\text{CF} = C \times \frac{1}{0.019 \text{ m}^2} \times \frac{1}{d} \quad (3)$$

where CF (mg C $\text{m}^{-2} \text{day}^{-1}$) is the carbon flux of the FPs or FLD cells, C is the total carbon content of individuals or cells in each sample, 0.019 m^2 is the mouth area of the trap, and d is the space between samples (2016: 4 days, 2019: 1 day, 2020: 6 days).

The trap samples were filtered using pre-combusted (450°C for 4 hr) Whatman GF/F filters for POC analyses. Filters were rinsed using a 0.25 mol L⁻¹ sodium thiosulfate solution, desalted by short washing with distilled water, and dried at 60°C. POC was measured using an elemental analyzer connected to an isotope-ratio mass spectrometer (Flash 2000-ConfloIV-DeltaV advantage, Thermo Scientific). POC fluxes were estimated by dividing the total mass per sample by the time interval and trap collection area.

2.9. Eukaryotic Community Structure Analysis

The ellipsoidal FPs (60 m depth: 7 ind.; 150 m depth: 7 ind.) and FLD cells (60 m depth: 10 cells; 150 m depth: 6 cells) were sorted randomly from the sinking particles sampled in January 2019. The nuclei of the FLD cells were removed from the cells using a stereomicroscope (Olympus SZX7, Olympus Inc.). The FPs and FLD cells were homogenized in 5% Chelex® 100 using a hand-held pestle homogenizer, and the solutions were incubated at 100°C for 20 min (Nagai et al., 2012; Peng et al., 2013).

The extracted DNA was used as a template for PCR amplification of the eukaryotic 18S rRNA gene using the eukaryotic universal primer set 1389F/1510R (Amaral-Zettler et al., 2009) (Table S2 in Supporting Information S1). Each 25 µL of the PCR mixture consisted of 2 µL of extracted DNA, 1.25 µL of 10 µmol·L⁻¹ of each primer, and 12.5 µL of 2 × PCR Master Mix. PCR amplification was performed via an initial denaturation at 94°C for 2 min, followed by 30 cycles of 10 s at 98°C, 30 s at 56°C, 30 s at 72°C, and a final extension at 68°C for 7 min. These amplicons were subsequently used as templates for indexing PCR to link the overhangs to Illumina sequencing adapters and indices for downstream sequencing. Each PCR mixture included 1 µL of amplicon, 1.25 µL of each of the index primers, 9 µL of diluted water, and 12.5 µL of 2 × PCR Master Mix. The PCR conditions followed were 94°C for 2 min, 8 cycles of 98°C for 10 s, 50°C or 59°C for 30 s, 68°C for 60 s, and a final extension at 68°C for 7 min. The PCR products were analyzed using a 2% agarose gel. Amplicons were cleaned and concentrated via silica column purification (NucleoSpin® Gel and PCR Clean-up, Macherey-Nagel, Germany), according to the manufacturer's instructions. The purified amplicons were pooled at equimolar concentrations.

2.10. High-Throughput Sequencing

The equimolar mix was sequenced using an Illumina MiSeq sequencing system at the Food Assessment & Management Center (FASMAC Co., Ltd., Japan). The quality of the demultiplexed raw sequences was analyzed using FastQC (v0.11.4; Babraham Bioinformatics). Unique sequences were aligned using Mothur software (version 1.43.0) against the Silva reference file version 138.1 (Schloss et al., 2009). Pre-clustering with a 1 bp mismatch allowance was performed to remove the pyrosequencing error (Huse et al., 2010). The aligned sequences were sorted using splitting abundance (cut-off = 10) to check for possible errors. Chimeric sequences were detected using UCHIME (USEARCH v.11; Edgar et al., 2011) and were removed. The remaining reads were clustered into operational taxonomic units (OTUs), which are units for the number of species determined by DNA sequence similarities between the reads. According to the furthest-neighbor distance, all singletons at 97% similarity, defined as an out composed of one single sequence that only occurs once in the whole analysis, were removed to avoid any possible errors induced by the sequencing process. The taxonomic groups “Mammalia,” “Archosauria,” “Hexapoda,” “Arachnida,” and “*Gyrodinium*” were removed from the target lineage to remove contamination and compare the contents between FLD cells and FPs without nucleic DNA of *Gyrodinium*.

2.11. Statistical Analysis

Statistical analyses were performed using the vegan, heatmap3, and ggplot2 packages of the software R v.4.1.2 (Oksanen et al., 2019; Villanueva & Chen, 2019; Zhao et al., 2014). Non-parametric multidimensional scaling (NMDS) and cluster analysis were based on the horn-Yamashita distance dissimilarity. Analysis of similarities (ANOSIM) was used to investigate the significance.

3. Results and Discussion

3.1. Morphological Features by Microscopic Observation

FLDs were sampled using time-series drifting sediment traps located in the seasonal ice zone of the Indian sector of the Southern Ocean during the austral summer (Figures S1 and S2 in Supporting Information S1).

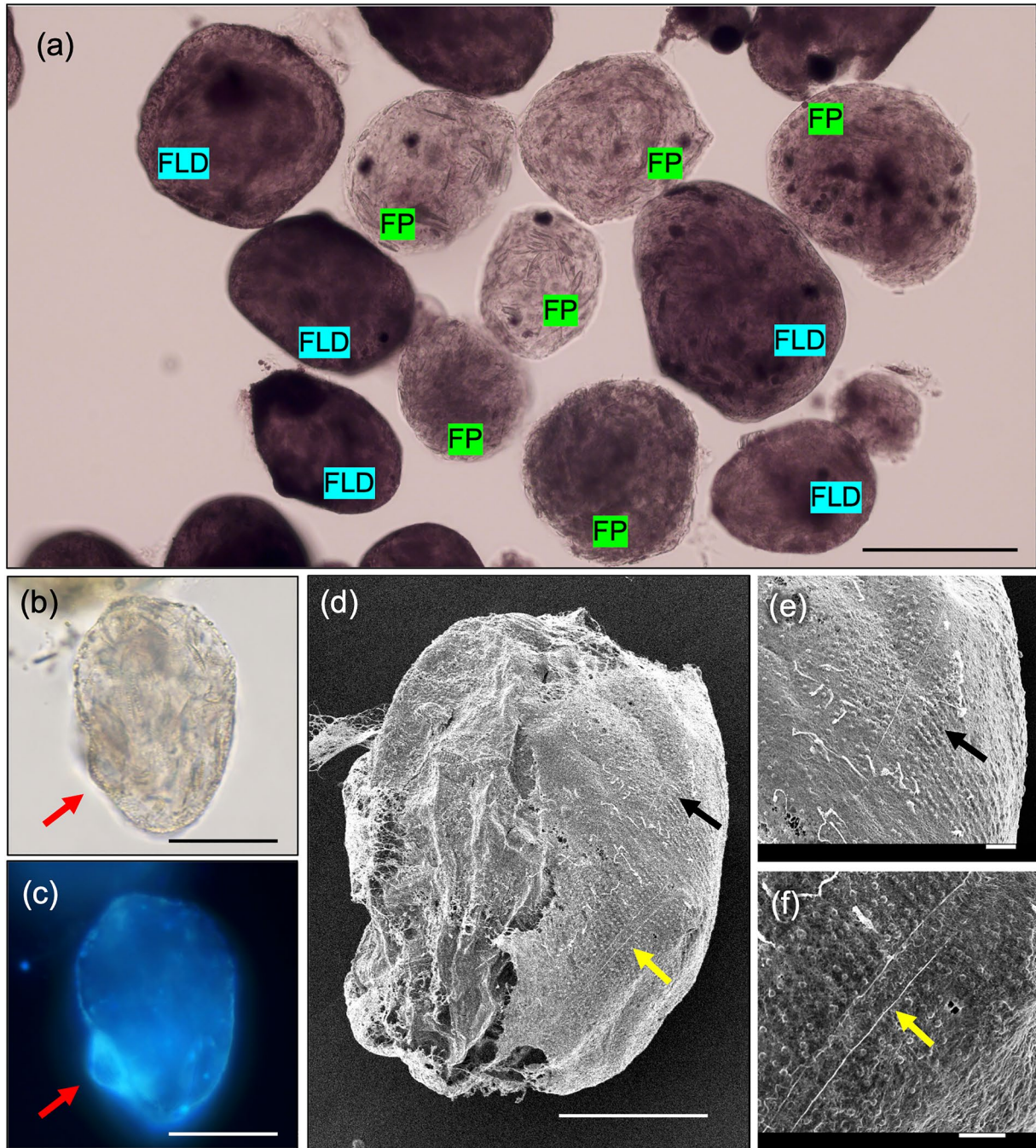


Figure 1. Microscopic observation of fecal pellet-like dinoflagellates (FLDs) and fecal pellets (FPs). (a) FLD cells and FPs among the sinking particles. (b, c) The cell and the cell stained with 4',6-diamidino-2-phenylindole are observed under light and fluorescence microscopes, respectively. The red arrow indicates the nucleus of the cell. (d–f) The cell sampled at 150 m depth using an electron microscope. Yellow and black arrows indicate the sulcus and spots, respectively. The left side of the cell collapsed due to manipulation for detritus removal and/or due to the dry-freezing method. Scale bar: (a–c) 200 μm , (d) 100 μm , and (e–f) 10 μm .

The appearance of FLDs was similar to that of spherical FPs (Figure 1a). The cells were oval and had an average size of $146 \pm 46 \mu\text{m} \times 192 \pm 59 \mu\text{m}$ ($n = 807$; Table 1). The size of the FLDs was $2.8 \times 10^6 \pm 2.7 \times 10^6 \mu\text{m}^3$ (Table 1), which was similar to that of the FPs of the copepods *Calanus finmarchicus* ($2.12 \times 10^6 \pm 0.82 \times 10^6 \mu\text{m}^3$; Svensen et al., 2012) and *Neocalanus cristatus* ($4.7 \times 10^6 \pm 8.9 \times 10^5 \mu\text{m}^3$; Stamieszkin et al., 2021). The nuclei of the cells were observed on the surface using DAPI staining (Figures 1b and 1c). A sulcus and spots, but no flagella, were observed on the cells using an electron microscope (Figures 1d–1f). Microscopic observations

Table 1
Diameter, Length, and Volume of Fecal Pellet-Like Dinoflagellate (FLD) Cells and Oval and/or Ellipsoidal Fecal Pellet (FP) Sampled in the Seasonal Ice Zone of the Southern Ocean

	FLD cells			Oval and/or ellipsoidal FPs		
	Diameter (μm)	Length (μm)	Volume (μm ³)	Diameter (μm)	Length (μm)	Volume (μm ³)
Average	146	192	2.8 × 10 ⁶	151	197	4.7 × 10 ⁶
Standard deviation	46	59	2.7 × 10 ⁶	76	95	1.8 × 10 ⁷
Median	143	188	2.1 × 10 ⁶	144	191	2.1 × 10 ⁶
Range	348	386	3.0 × 10 ⁷	889	1,111	4.8 × 10 ⁸
Minimum	35	36	2.2 × 10 ⁴	11	31	1.9 × 10 ³
Maximum	382	422	3.0 × 10 ⁷	900	1,143	4.8 × 10 ⁸

indicated that the FLD cells were dinoflagellates >100 μm in diameter having a sulcus and spots. Based on these morphological features (nuclei, sulcus, and spots), FLDs and oval FPs could be distinguished.

3.2. Identification of FLDs at the Species Level Using 18S rRNA Gene Sequencing

To identify the FLDs at the species level, their taxonomic and phylogenetic statuses were examined using the 18S rRNA gene sequences. The obtained sequences from all cells were divided into two major groups. The sequence similarity between the groups was 97%, and the genetic distance ranged from 0.021 to 0.023. The groups were clustered with *Gyrodinium rubrum* (AB120003.1) or *Gyrodinium heterogrammum* (KP790159.1), respectively (Figure 2). Sixty-four of the 66 cells collected from a depth of 60 m in the austral summers of 2019 and 2020 were identified as *G. rubrum*, and the remaining two were identified as *G. heterogrammum*. Conversely, 20 of the 22 cells collected from a depth of 150 m in the austral summers of 2019 and 2020 were identified as *G. heterogrammum*, and the remaining two were identified as *G. rubrum*.

G. rubrum cells sampled in Otaru Bay of Japan have a cell size of 35.8–63.2 μm in diameter and 84.9–140.4 μm in length ($n = 8$) (Takano & Horiguchi, 2004). *G. heterogrammum* cells sampled in Port Phillip Bay of Australia were 24–30 μm in diameter and 32–35 μm in length ($n = 16$; Larsen, 1994). In contrast, the FLD cell sizes are distinctively larger than the reported *Gyrodinium* cell sizes (Larsen, 1994; Takano & Horiguchi, 2004). Large *Gyrodinium* cells have been reported in previous studies (Buck et al., 2005; Gómez et al., 2020; Saito et al., 2006). Field observation in the North Pacific Ocean reported that *Gyrodinium* sp. fed on diatom chains with sizes up to 12 times their length ($1.99 \times 10^5 \mu\text{m}^3$ in volume) after a diatom bloom (Saito et al., 2006). A previous study reported that an athecate phagotrophic dinoflagellate (*Gyrodinium* sp.) ingested chain-forming diatoms and was abundant in Monterey Bay, California (Buck et al., 2005). Large *G. spirale* were observed in the North Sea after a *Phaeocystis* bloom (Gómez et al., 2020). Taken together, the FLD cells (large *G. rubrum* cells and *G. heterogrammum* cells) observed were likely to be hypertrophied cells stuffed with prey.

3.3. FLD Cells Were Oval Pellet Producers Not Minipellet Producers

Gyrodinium species also produce diatom-containing minipellets (Buck & Newton, 1995; Saito et al., 2006). Interestingly, during manipulation using a microneedle under a microscope, an object similar to an oval FP emerged from an FLD cell (Movie S1). This finding suggests that FLD cells excrete oval FPs with a 100–300 μm diameter. The FPs emerging from FLD cells were larger than the minipellets generated by *Gyrodinium* (Buck & Newton, 1995; Saito et al., 2006). If FLD cells live and generate oval pellets, their FPs may be more effective carbon carriers than the reported minipellets (Buck et al., 2005; Saito et al., 2006). To confirm whether oval FPs were excreted by FLD cells, their flux correlation and eukaryotic community structures were investigated.

The FLD cells and oval or ellipsoidal FPs in the sinking particle samples were counted, and their diameters, lengths, and fluxes were measured and calculated. The diameter and length of oval or ellipsoidal FPs were 151 ± 76 and 197 ± 95 μm, respectively (Table 1). We investigated the correlation between the flux of oval or ellipsoidal FPs (excluding those whose size exceeded the 95% confidence level of the cell size of FLDs for either

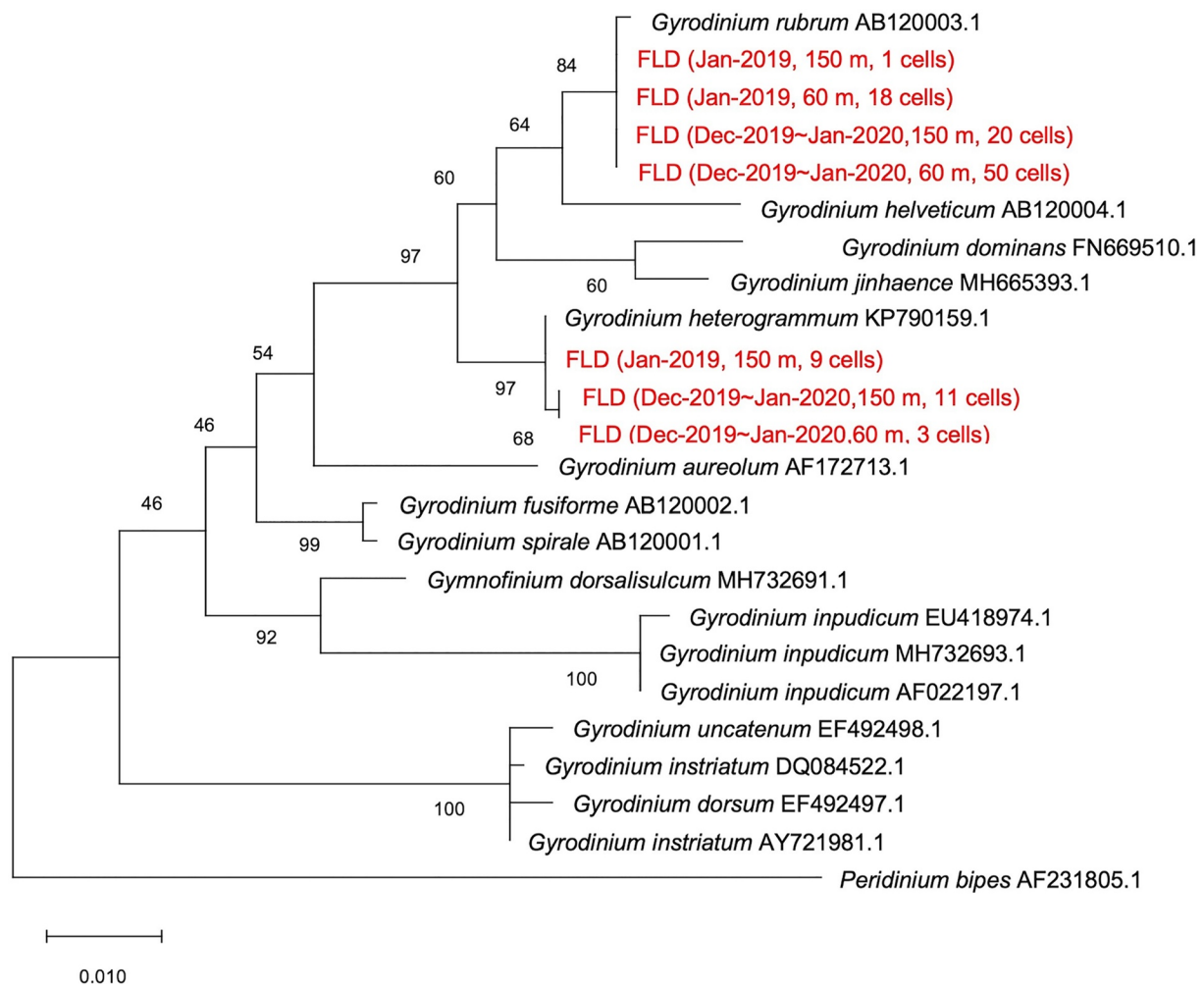


Figure 2. Neighbor-joining phylogenetic tree of the genus *Gyrodinium* based on the partial 18S rRNA gene sequences. GenBank accession numbers are provided. Bar: 0.01 substitutions per nucleotide position. Numbers at the nodes indicate the bootstrap probabilities (among 1,000 samples). The red text corresponds to the Fecal pellet-like dinoflagellates (FLD) samples.

the diameter or length) and the flux of FLD cells; a strong positive correlation ($R^2 = 0.81$) was observed between the flux of FPs (considered as FLD's FP based solely on size, not morphological features) and the flux of FLD cells (Figure S3a in Supporting Information S1). The correlations between the flux of FLDs and the flux of FPs that were smaller and larger than the FLD size based on the 95% confidence level were 0.63 and 0.67, respectively (Figures S3b and S3c in Supporting Information S1). These values were lower than the correlation between the flux of FPs generated by FLDs and the flux of FLD cells. These results support the hypothesis that the FLDs produced these oval FPs. To confirm this, the eukaryotic community structures in the food vacuoles of FLD cells (16 cells) and the contents of the oval and/or ellipsoidal FPs (14 individuals) were analyzed and compared. A total of 2,522,738 reads of the 18S rRNA (V9 region) gene were obtained and clustered into 738 OTUs with 97% similarity, of which 317 were shared OTUs. The FLD cells had 312 specific OTUs, whereas the FPs had 109 specific OTUs. The differences in eukaryotic community structures were analyzed using NMDS based on OTU composition (Figure S4 in Supporting Information S1). The 95% confidence interval between the FLD cells and FPs overlapped, and no significant difference was observed (ANOSIM, $p = 0.09$). The differences in eukaryotic community structures between the FLD cells and FPs were also visualized using a cluster map (Figure 3). The most abundant species were *Fragilariopsis sublineata*, uncultured Dinophyceae, and Thoracosphaeraceae. Four major clusters were formed due to differences in the eukaryotic community structure between FLDs and FPs. In samples where *Fragilariopsis sublineata* was relatively abundant, no apparent differences in eukaryotic community structure were observed between the prey in the food vacuoles of FLD cells and the contents of ellipsoidal

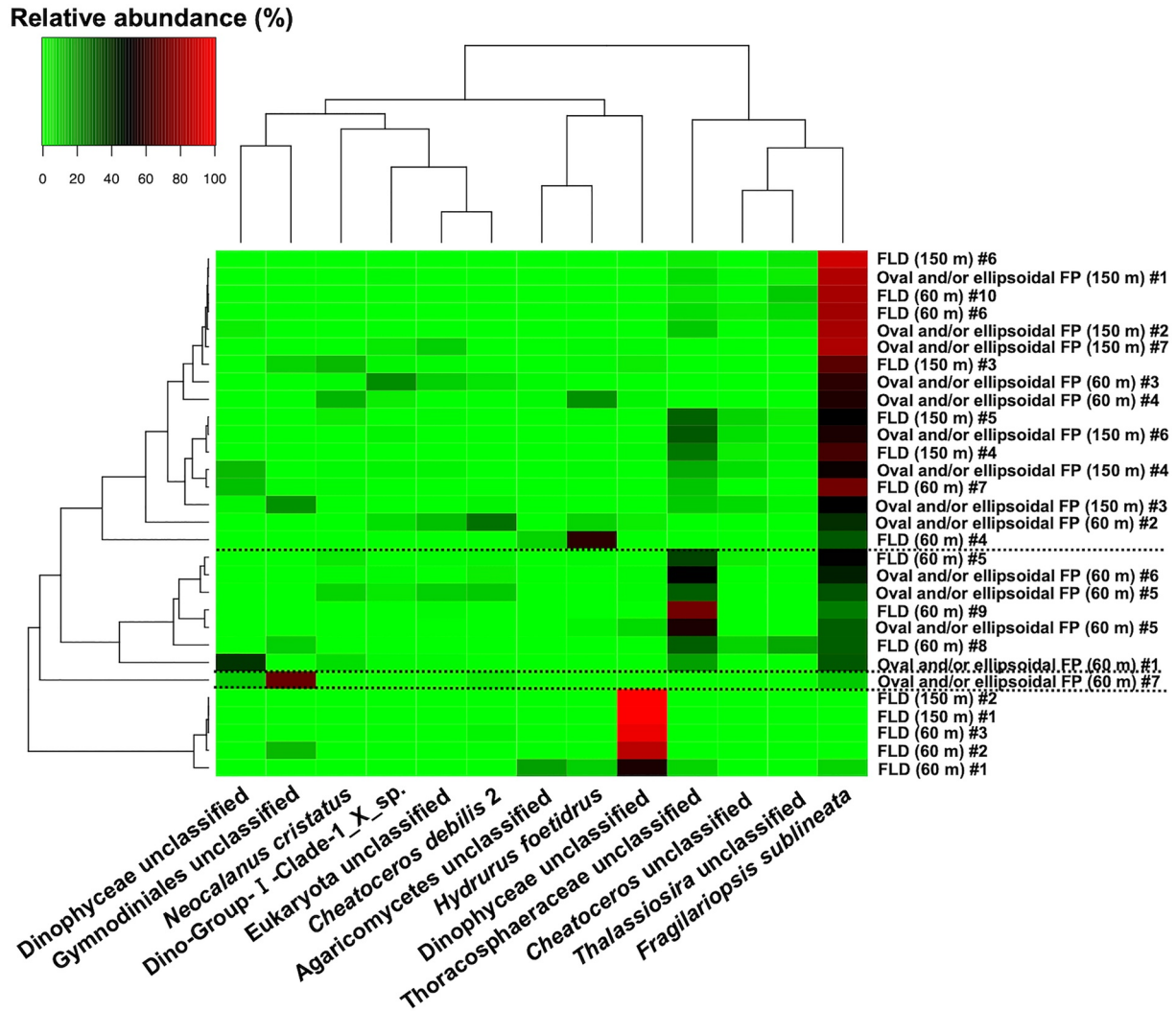


Figure 3. Comparison between fecal pellet-like dinoflagellates (FLDs) and oval or ellipsoidal fecal pellets (FPs). Heatmap of taxonomic species composition. The heatmap represents relative abundance of the abundant taxonomic species (>1%). Both the taxa and the samples were clustered. Color intensity in the cluster dendrogram corresponds to the relative abundance.

Table 2
Sinking Velocity of Fecal Pellet-Like Dinoflagellate Cells Using Reported Density of Fecal Pellets (FPs), Cysts, and Living Cells

	FP ^a	Cyst ^b	Living cell ^c
Average	202	102	57
Standard deviation	178	90	50
Median	126	63	35
Range	1,152	582	322
Minimum	10	4.8	2.7
Maximum	1,161	586	325

^aDensity value for sphere FP used: 1.19 g cm⁻³ (Atkinson et al., 2012). ^bDensity value for *Gyrodinium* cyst used: 1.14 g cm⁻³ (Anderson et al., 1985). ^cDensity value for living *Gyrodinium* cell used: 1.09 g cm⁻³ (Kamykowski et al., 1992).

FPs. These results suggest that the sinking particles captured by the sediment trap, which included oval or ellipsoidal FPs, also contained FPs produced by FLDs.

3.4. Sinking Rate of FLD Cells Based On Stokes' Law

The sinking rates of the FLD cells were examined using Stokes' law. The reported densities for living *Gyrodinium* cells, *Gyrodinium* cysts, and FPs were used as the FLD density (Table 2; Figure 4a). If FLD cells were live, the average sinking rate of the FLD cells was 57 ± 35 m day⁻¹ (range: 2.7–325 m day⁻¹; Table 2). The maximum and average values were higher than those of the *Gyrodinium* cells sampled in Monterey Bay, California, in the North Pacific (Buck et al., 2005; Saito et al., 2006). These values were also higher than the sinking rates of various phytoplankton (Bach et al., 2012). If FLD cells were cysts, the average sinking rate of the FLD cells was 102 ± 63 m day⁻¹ (range: 4.8–586 m day⁻¹; Table 2). This value

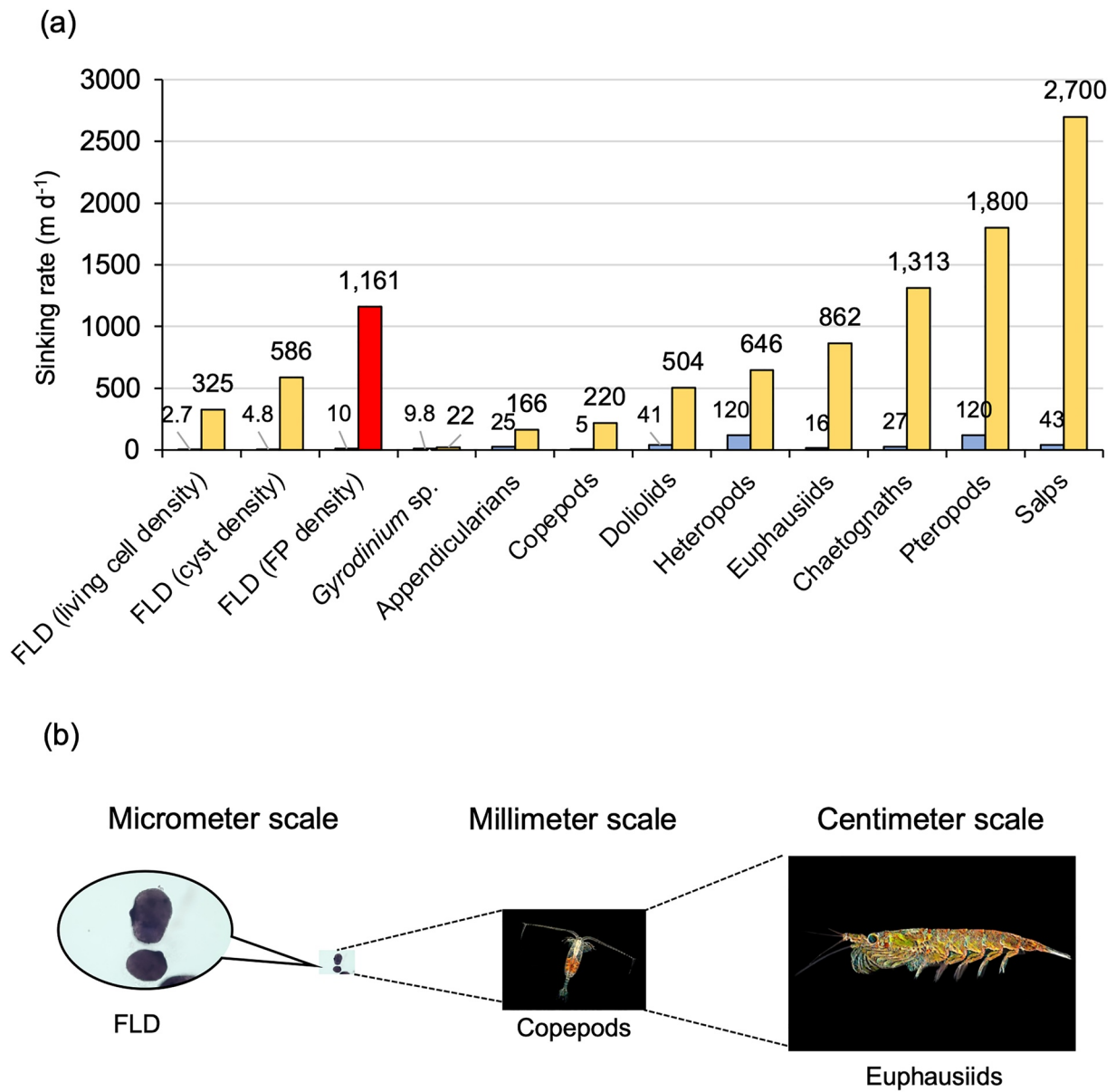


Figure 4. Differences in the sinking rate and a schematic diagram of cell or body sizes. (a) The sinking rate of the fecal pellets (FPs) produced by metazoans and protozoa (Buck et al., 2005; Saito et al., 2006; Turner, 2002, 2015). Fecal pellet-like dinoflagellate (FLD) sinking rates were calculated using three densities: those of living cells, cysts, and FPs. The light yellow and blue bars indicate the maximum and minimum sinking rates, respectively. The red bar indicates the maximum sinking rate of FLDs. The sinking rate of FLDs was estimated based on Stokes' law. (b) Schematic diagram of the differences in cell or body size between euphausiids, copepods, and FLDs.

was 9–17 times higher than the sinking rate of dinoflagellate cysts (Anderson et al., 1985). At least, the average sinking rate of FLD could be higher than that of other protozoa and dinoflagellate cysts, irrespective of whether the FLDs were living cells or cysts.

If the density of FLD was the same as that of FP, the average FLD sinking rate was $202 \pm 126 \text{ m day}^{-1}$ (range: 10–1,161 m day^{-1} ; Table 2). Surprisingly, the maximum sinking rate of FLD cells was higher than those of copepod- and euphausiid-produced FPs, although the FLD cells were smaller than the metazoans (Figure 4b). The sinking rates of the FPs produced by Antarctic krill and salps in the Antarctic Peninsula were 233.4 ± 154.3 and $586.0 \pm 692.0 \text{ m day}^{-1}$, respectively (Pauli et al., 2021). The sinking rate of large copepod FPs sampled in the northeastern tropical Atlantic was $115.9 \pm 52.6 \text{ m day}^{-1}$, according to Stokes's law (Yoon et al., 2001). The FLD average sinking rate was comparable to that of the Antarctic krill FPs sampled in the Antarctic Peninsula (Pauli

et al., 2021). The sinking rate of the FPs generated by the FLD cells was comparable to that of the FLD cells, assuming that the size of the FPs was similar to the FLD cell size. If their FPs have a high density, they will likely function as carbon carriers, as effective as the metazoan FPs, owing to their high sinking rate.

3.5. Flux of FLD Cells Examined Using Various Carbon Conversion Factors

If FLDs are cysts or dead cells, their carbon flux could be due to passive sinking. In contrast, if FLDs are living cells, they can descend and ascend, so the abundance in traps might not be a passive sinking flux. However, the FP generated by FLD cells might be through passive sinking flux. Therefore, it is essential to consider the status of FLD cells when estimating their carbon flux. *Gyrodinium* cysts have two transparent layers (Kobayashi et al., 2001; Kojima & Kobayashi, 1992; Moestrup et al., 2014). Although the outer transparent layer could collapse during sampling, no outer layer on FLD cells (*G. rubrum* and *G. heterogrammum*) was observed. Moreover, it was thought that there is no need to resist starvation because phytoplankton, such as diatoms, were observed inside the cells (Figure S5 in Supporting Information S1). At least, FLD cells were not considered to be cysts. Although there was no certainty as to whether the FLDs are living cells, the range of FLD carbon fluxes was estimated using various carbon conversion factors for dinoflagellate cells and oval FPs (Archer et al., 1996; Gleiber et al., 2012; Manno et al., 2015; Menden-Deuer & Lessard, 2000; Nakamura et al., 1992; Rembauville et al., 2015) (Tables 3 and 4). The ranges of FLD carbon flux were 0.0046 to 16 mgC m⁻² day⁻¹ using the conversion factor for heterotrophic dinoflagellate cells (Menden-Deuer & Lessard, 2000), 0.0046 to 12 mgC m⁻² day⁻¹ using the conversion factor for total dinoflagellate cells (Menden-Deuer & Lessard, 2000), and 0.0029 to 25 mgC m⁻² day⁻¹ using the conversion factor for *G. dominans* cells (Archer et al., 1996; Nakamura et al., 1992). The maximum FLD carbon flux/the total POC flux was 45%, 32%, and 78%, respectively. If the FLD cells were dead, their passive flux could contribute to a maximum of 12 mgC m⁻² day⁻¹ (32% of total POC flux). In contrast, if FLD cells were alive, not all cells would be sequestered in the deep ocean because they could sink and ascend owing to cell size changes due to feeding and excretion. In other words, if FLD cell flux was not a passive sinking flux, a maximum of 32% of total POC flux might be overestimated. Although the flux of FP generated by FLD cells could form an additional flux, this flux was not estimated because of little information on their FP (only the size was known). Further studies on FLD will be needed to reveal their contribution to carbon export.

As previously described, FLD cells might be overlooked in POC export evaluations because their appearance was similar to that of oval FPs. If carbon conversion factors of oval FPs were used for estimation of FLD flux, the ranges of FLD carbon flux were 0.0018 to 16 mgC m⁻² day⁻¹ using the conversion factor for total FP including oval and spherical FPs (Rembauville et al., 2015), 0.0021 to 18 mgC m⁻² day⁻¹ using the conversion factor for FPs sampled from austral autumn to summer of the Scotia Sea in the Southern Ocean (Manno et al., 2015), and 0.0019 to 17 mgC m⁻² day⁻¹ using the conversion factor for FPs sampled in the Western Antarctic Peninsula (Gleiber et al., 2012). The maximum values of the FLD carbon flux/the total POC flux obtained using three carbon conversion factors were 56%, 53%, and 63%, respectively. Carbon fluxes of oval or ellipsoidal FPs were also estimated using carbon conversion factors (Manno et al., 2015) (Table S3 in Supporting Information S1). The oval or ellipsoidal FP carbon flux ranged from 0.14 to 56 mgC m⁻² day⁻¹. If FLD cells were considered as FP and their flux was estimated in the same manner as FP flux, the FP carbon flux may be overestimated by a maximum of 18 mgC m⁻² day⁻¹. The contributions of FLD cells and their oval FP are unknown because no information is available on whether FLD cells are alive or dead. However, at least the contributions of FLD cells and oval FPs to carbon export were found to differ. Therefore, distinguishing between FLD cells and oval or ellipsoidal FPs among sinking particles is essential for accurately estimating POC flux.

4. Conclusion

In this study, we reported on FLDs captured by drifting sediment traps in the east Antarctic seasonal ice zone. The FLD cells were identified at the species level, and their FPs as well as FLD carbon flux were investigated. The current results indicate that FLDs were (a) heterotrophic dinoflagellates *G. rubrum* and *G. heterogrammum*, (b) producers of larger oval FPs than minipellets, and (c) potential contributors to carbon export.

In biogeochemical cycle research and future predictions for carbon sequestration, metazoans such as Antarctic krill and copepods have been highlighted due to their high biomass and considerable contribution to carbon export (Cavan et al., 2019; Flores et al., 2012). Our results suggest that FLDs serve as potential drivers for

Table 3
Variation in Fecal Pellet-Like Dinoflagellate (FLD) Carbon Flux Using Three Conversion Factors for Dinoflagellate Cells

Date	Depth (m)	POC flux (mgC m ⁻² day ⁻¹)	FLD flux (HDF) (mgC m ⁻² day ⁻¹) ^a	FLD flux (TDF) (mgC m ⁻² day ⁻¹) ^b	FLD flux (Gd) (mgC m ⁻² day ⁻¹) ^c
10–13 December 2016	50	25	7.1	4.9	14
14–17 December 2016		62	16	12	25
18–21 December 2016		30	14	9.7	24
22–25 December 2016		11	0.19	0.16	0.23
26–29 December 2016		17	1	0.79	1.5
30 December 2016 to 2 January 2017		10	2.7	2	4.6
3–8 January 2017		13	2.2	1.6	3.6
14–15 January 2019	60	39	3.9	2.8	6.2
15–16 January 2019		34	n.d.	n.d.	n.d.
16–17 January 2019		26	4.2	3.1	6.4
17–18 January 2019		57	5	3.8	7.1
18–19 January 2019		35	2.2	1.6	3.4
19–19 January 2019		96	5.7	4.5	7.4
14–15 January 2019	150	6.4	0.82	0.65	1
15–16 January 2019		13	0.11	0.1	0.089
16–17 January 2019		17	0.1	0.092	0.088
17–18 January 2019		25	0.81	0.68	0.87
18–19 January 2019		27	0.83	0.65	1.1
19–19 January 2019		130	1.2	1	1.2
10–15 December 2019	60	70	n.d.	n.d.	n.d.
16–21 December 2019		100	1.8	1.4	2.5
22–27 December 2019		87	3.5	2.6	5.2
28 December 2019 to 2 January 2020		62	3.5	2.7	5.3
3–8 January 2020		38	0.31	0.25	0.39
9–14 January 2020		91	0.61	0.51	0.7
15–20 January 2020		39	3.7	2.8	5.7
10–15 December 2019	150	17	0.0046	0.0046	0.0029
16–21 December 2019		150	n.d.	n.d.	n.d.
22–27 December 2019		160	0.0089	0.0085	0.0068
28 December 2019 to 2 January 2020		53	0.0049	0.0049	0.0031
3–8 January 2020		29	0.0071	0.0068	0.0052
9–14 January 2020		100	0.047	0.04	0.051
15–20 January 2020		29	0.18	0.14	0.21

Note. “n.d.” indicates no detection.

^aConversion factor for heterotrophic dinoflagellate (HDF) cells used (Menden-Deuer & Lessard, 2000). ^bConversion factor for total dinoflagellate (TDF) cells used (Menden-Deuer & Lessard, 2000). ^cConversion factor for *Gyrodinium dominans* (Gd) cell used (Archer et al., 1996; Nakamura et al., 1992).

biological carbon pumps, although heterotrophic dinoflagellates have garnered considerable attention in studies on carbon flux estimation because they are thought to act as POC and DOC consumers in the microbial loop, contributing to carbon flux attenuation. FLDs have not been considered in models such as the Biogeochemical Elemental Cycle model embedded in the Community Earth System Model and the Regulated Ocean Ecosystem Model (Danabasoglu et al., 2020; Hauck et al., 2013; Schourup-Kristensen et al., 2014). Moreover, the response of *Gyrodinium* species to future climate changes due to global warming and ocean acidification

Table 4
Variation in Fecal Pellet-Like Dinoflagellate (FLD) Carbon Flux Using Conversion Factor for Fecal Pellets

Date	Depth (m)	POC flux (mgC m ⁻² day ⁻¹)	FLD flux (0.052) (mgC m ⁻² day ⁻¹) ^a	FLD flux (0.041) (mgC m ⁻² day ⁻¹) ^b	FLD flux (0.038) (mgC m ⁻² day ⁻¹) ^c
10–13 December 2016	50	25	13	10	9.5
14–17 December 2016		62	23	18	17
18–21 December 2016		30	22	17	16
22–25 December 2016		11	0.21	0.17	0.16
26–29 December 2016		17	1.4	1.1	1
30 December 2016 to 2 January 2017		10	4.3	3.4	3.1
3–8 January 2017		13	3.4	2.7	2.5
14–15 January 2019	60	39	5.7	4.5	4.2
15–16 January 2019		34	n.d.	n.d.	n.d.
16–17 January 2019		26	6	4.7	4.3
17–18 January 2019		57	6.6	5.2	4.8
18–19 January 2019		35	3.2	2.5	2.3
19 January 2019		96	6.9	5.5	5.1
14–15 January 2019	150	6.4	0.95	0.75	0.69
15–16 January 2019		13	0.082	0.065	0.06
16–17 January 2019		17	0.081	0.064	0.06
17–18 January 2019		25	0.81	0.64	0.59
18–19 January 2019		27	1.0	0.81	0.75
19 January 2019		130	1.1	0.87	0.8
10–15 December 2019	60	70	n.d.	n.d.	n.d.
16–21 December 2019		100	2.3	1.8	1.7
22–27 December 2019		87	4.8	3.8	3.5
28 December 2019 to 2 January 2020		62	5.0	3.9	3.6
3–8 January 2020		38	0.36	0.28	0.26
9–14 January 2020		91	0.65	0.51	0.47
15–20 January 2020		39	5.3	4.2	3.8
10–15 December 2019	150	17	0.0027	0.0021	0.0019
16–21 December 2019		150	n.d.	n.d.	n.d.
22–27 December 2019		160	0.0063	0.005	0.0046
28 December 2019 to 2 January 2020		53	0.0029	0.0023	0.0021
3–8 January 2020		29	0.0048	0.0038	0.0035
9–14 January 2020		100	0.047	0.037	0.035
15–20 January 2020		29	0.20	0.16	0.15

Note. “n.d.” indicates no detection.

^aConversion factor for ovoid pellets in the Scotia Sea (Manno et al., 2015). ^bConversion factor for ovoid pellets in the Western Antarctic Peninsula (Gleiber et al., 2012). ^cConversion factor for total fecal pellets (Rembauville et al., 2015).

has not been clarified. A better understanding of the physiological and ecological roles of two described *Gyrodinium* species will be urgently required in future predictions of carbon sequestration in the Southern Ocean.

Conflict of Interest

The authors declare no conflicts of interest relevant to this study.

Data Availability Statement

DNA data for the 18S rRNA gene of FLDs generated in this study are available in DDBJ/EMBL/GenBank (Accession number: LC732348–LC732435, <https://www.ncbi.nlm.nih.gov>). The high-throughput DNA sequencing data are available in the DNA Data Bank of Japan DDBJ SRA (Accession number: DRR415046–DRR415075, <https://ddbj.nig.ac.jp/search>). The size, sinking rate, and flux of FLD and zooplankton FP data that support the findings of this study are available in the Arctic Data Archive System, managed by the Research Organization of Information and Systems, Polar Environment Data Science Center, National Institute of Polar Research, Japan (<https://doi.org/10.17592/001.2022102001>). Source data for NMDS analysis and cluster map are available in a GitHub repository (https://github.com/Ryo-Matsuda-17/Matsuda_et_al_2023_JGR_BG).

Software Availability Statement: Phylogenetic tree and other figures were made using MEGA 7 (<https://www.megasoftware.net>) and R version 4.1.2 (<https://www.r-project.org>). Analysis of high-throughput DNA sequence data was performed using Mothur (<https://mothur.org>). R code for NMDS analysis and cluster map is available in a GitHub repository (https://github.com/Ryo-Matsuda-17/Matsuda_et_al_2023_JGR_BG).

Acknowledgments

We would like to express our gratitude to the late Dr. T. Odate from the National Institute of Polar Research, who passed away in February 2021, for providing us with the opportunity to conduct our observations. We also extend our thanks to the captain and crew of the icebreaker *Shirase* and the TV *Umitaka-maru* for their support during the cruises. Special thanks are offered to Dr. M. Yamamoto-Kawai for her valuable comments on the study results. We would also like to acknowledge A. Kagesawa, S. Okano, and J. Han for their technical assistance during the experiments. This work was supported by the Japan Society for the Promotion of Science KAKENHI (Grants 17H06319 to M. Moteki, 17K07579 and 20H04313 to R. Makabe, and 23KJ2057 to R. Matsuda), the Research Project Funds of the National Institute of Polar Research (Grant KP-308 to T. Odate), the Japanese Antarctic Research Expedition (Grant AP-0939 to M. Moteki), the Sasakawa Scientific Research (Grant 2021-4085 to R. Matsuda) from the Japan Science Society, and the Japan Science and Technology Society (Support for Pioneering Research Initiated by the Next Generation [SPRING]; Grant JPMJSP2143).

References

- Amaral-Zettler, L. A., McCliment, E. A., Ducklow, H. W., & Huse, S. M. (2009). A method for studying protistan diversity using massively parallel sequencing of V9 hypervariable regions of small-subunit ribosomal RNA Genes. *PLoS One*, *4*(7), 1–9. <https://doi.org/10.1371/journal.pone.0006372>
- Anderson, D. M., Lively, J. J., Reardon, E. M., & Price, C. A. (1985). Sinking characteristics of dinoflagellate cysts. *Limnology & Oceanography*, *30*(5), 1000–1009. <https://doi.org/10.4319/lo.1985.30.5.1000>
- Archer, S. D., Leakey, R. J. G., Burkill, P. H., & Sleight, M. A. (1996). Microbial dynamics in coastal waters of East Antarctica: Herbivory by heterotrophic dinoflagellates. *Marine Ecology Progress Series*, *139*(1–3), 239–255. <https://doi.org/10.3354/meps139239>
- Atkinson, A., Schmidt, K., Fielding, S., Kawaguchi, S., & Geissler, P. A. (2012). Variable food absorption by Antarctic krill: Relationships between diet, egestion rate and the composition and sinking rates of their fecal pellets. *Deep-Sea Research Part II Topical Studies in Oceanography*, *59*–60, 147–158. <https://doi.org/10.1016/j.dsr2.2011.06.008>
- Bach, L. T., Riebesell, U., Sett, S., Febiri, S., Rzepka, P., & Schulz, K. G. (2012). An approach for particle sinking velocity measurements in the 3–400 μm size range and considerations on the effect of temperature on sinking rates. *Marine Biology*, *159*(8), 1853–1864. <https://doi.org/10.1007/s00227-012-1945-2>
- Bathmann, U. V., Noji, T. T., & von Bodungen, B. (1990). Copepod grazing potential in late winter in the Norwegian Sea—A factor in the control of spring phytoplankton growth? *Marine Ecology Progress Series*, *60*(3), 225–233. <https://doi.org/10.3354/meps060225>
- Beaumont, K. L., Nash, G. V., & Davidson, A. T. (2002). Ultrastructure, morphology and flux of microzooplankton faecal pellets in an east Antarctic fjord. *Marine Ecology Progress Series*, *245*, 133–148. <https://doi.org/10.3354/meps245133>
- Beaumont, K. L., Plummer, A. J., Hosie, G. W., & Ritz, D. A. (2001). Production and fate of faecal pellets during summer in an East Antarctic fjord. *Hydrobiologia*, *453*–454, 55–65. <https://doi.org/10.1023/A:1013103630883>
- Buck, K. R., Bolt, P. A., & Garrison, D. L. (1990). Phagotrophy and fecal pellet production by an athecate dinoflagellate in Antarctic sea ice. *Marine Ecology Progress Series*, *60*(1), 75–84. <https://doi.org/10.3354/meps060075>
- Buck, K. R., Marin, R., III, & Chavez, F. P. (2005). Heterotrophic dinoflagellate fecal pellet production: Grazing of large, chain-forming diatoms during upwelling events in Monterey Bay, California. *Aquatic Microbial Ecology*, *40*(3), 293–298. <https://doi.org/10.3354/ame040293>
- Buck, K. R., & Newton, J. (1995). Fecal pellet flux in Dabob Bay during a diatom bloom: Contribution of microzooplankton. *Limnology & Oceanography*, *40*(2), 306–315. <https://doi.org/10.4319/lo.1995.40.2.0306>
- Cavan, E. L., Belcher, A., Atkinson, A., Hill, S. L., Kawaguchi, S., McCormack, S., et al. (2019). The importance of Antarctic krill in biogeochemical cycles. *Nature Communications*, *10*(1), 1–13. <https://doi.org/10.1038/s41467-019-12668-7>
- Danabasoglu, G., Lamarque, J. F., Bacmeister, J., Bailey, D. A., DuVivier, A. K., Edwards, J., et al. (2020). The Community Earth System Model Version 2 (CESM2). *Journal of Advances in Modeling Earth Systems*, *12*(2), 1–35. <https://doi.org/10.1029/2019MS001916>
- Dilling, L., & Alldredge, A. L. (1993). Can chaetognath fecal pellets contribute significantly to carbon flux? *Marine Ecology Progress Series*, *92*(1–2), 51–58. <https://doi.org/10.3354/meps092051>
- Edgar, R. C. (2004). MUSCLE: A multiple sequence alignment method with reduced time and space complexity. *BMC Bioinformatics*, *5*, 1–19. <https://doi.org/10.1186/1471-2105-5-113>
- Edgar, R. C., Haas, B. J., Clemente, J. C., Quince, C., & Knight, R. (2011). UCHIME improves sensitivity and speed of chimera detection. *Bioinformatics*, *27*(16), 2194–2200. <https://doi.org/10.1093/bioinformatics/btr381>
- Flores, H., Atkinson, A., Kawaguchi, S., Krafft, B. A., Milinevsky, G., Nicol, S., et al. (2012). Impact of climate change on Antarctic krill. *Marine Ecology Progress Series*, *458*, 1–19. <https://doi.org/10.3354/meps09831>
- Gleiber, M. R., Steinberg, D. K., & Ducklow, H. W. (2012). Time series of vertical flux of zooplankton fecal pellets on the continental shelf of the western Antarctic Peninsula. *Marine Ecology Progress Series*, *471*, 23–36. <https://doi.org/10.3354/meps10021>
- Gómez, F., Artigas, L. F., & Gast, R. J. (2020). Phylogeny and synonymy of *Gyrodinium heterostriatum* comb. nov. (Dinophyceae), a common unarmored dinoflagellate in the world oceans. *Acta Protozoologica*, *59*(2), 77–87. <https://doi.org/10.4467/16890027AP.20.007.12675>
- Gonzalez, H. E. (1992). Distribution and abundance of minipellets around the Antarctic Peninsula. Implications for protistan feeding behaviour. *Marine Ecology Progress Series*, *90*(3), 223–236. <https://doi.org/10.3354/meps090223>
- Gowing, M. M., & Silver, M. W. (1985). Minipellets: A new and abundant size class of marine fecal pellets. *Journal of Marine Research*, *43*(2), 395–418. <https://doi.org/10.1357/002224085788438676>
- Hauck, J., Völker, C., Wang, T., Hoppema, M., Losch, M., & Wolf-Gladrow, D. A. (2013). Seasonally different carbon flux changes in the Southern Ocean in response to the southern annular mode. *Global Biogeochemical Cycles*, *27*(4), 1236–1245. <https://doi.org/10.1002/2013GB004600>
- Honjo, S., Eglinton, T. I., Taylor, C. D., Ulmer, K. M., Sievert, S. M., Bracher, A., et al. (2014). The role of the biological pump in the global carbon cycle understanding an imperative for ocean science. *Oceanography*, *27*(3), 10–16. <https://doi.org/10.5670/oceanog.2014.78>
- Huse, S. M., Welch, D. M., Morrison, H. G., & Sogin, M. L. (2010). Ironing out the wrinkles in the rare biosphere through improved OTU clustering. *Environmental Microbiology*, *12*(7), 1889–1898. <https://doi.org/10.1111/j.1462-2920.2010.02193.x>

- IPCC. (2007). Climate change: Mitigation. Contribution of Working Group III to the Fourth Assessment Report of the Intergovernmental Panel on Climate Change. Cambridge University Press.
- Kamykowski, D., Reed, R. E., & Kirkpatrick, G. J. (1992). Comparison of sinking velocity, swimming velocity, rotation and path characteristics among six marine dinoflagellate species. *Marine Biology*, *113*(2), 319–328. <https://doi.org/10.1007/BF00347287>
- Klindworth, A., Pruesse, E., Schweer, T., Peplies, J., Quast, C., Horn, M., & Glöckner, F. O. (2013). Evaluation of general 16S ribosomal RNA gene PCR primers for classical and next-generation sequencing-based diversity studies. *Nucleic Acids Research*, *41*(1), 1–11. <https://doi.org/10.1093/nar/gks808>
- Kobayashi, S., Kojima, N., Itakura, S., Imai, I., & Matsuoka, K. (2001). Cyst morphology of a chain-forming unarmored dinoflagellate *Gyrodinium impudicum* Fraga et Bravo. *Phycological Research*, *49*(1), 61–65. <https://doi.org/10.1046/j.1440-1835.2001.00223.x>
- Kojima, N., & Kobayashi, S. (1992). Motile cell-like cyst of *Gyrodinium instriatum* Freudenthal et Lee (Dinophyceae). *Review of Palaeobotany and Palynology*, *74*(3–4), 239–247. [https://doi.org/10.1016/0034-6667\(92\)90009-6](https://doi.org/10.1016/0034-6667(92)90009-6)
- Komar, P. D., Morse, A. P., Small, L. F., & Fowler, S. W. (1981). An analysis of sinking rates of natural copepod and euphausiid fecal pellets. *Limnology & Oceanography*, *26*(1), 172–180. <https://doi.org/10.4319/lo.1981.26.1.0172>
- Kumar, S., Stecher, G., & Tamura, K. (2016). MEGA7: Molecular Evolutionary Genetics Analysis Version 7.0 for Bigger Datasets [Software]. *Molecular Biology and Evolution*, *33*(7), 1870–1874. <https://doi.org/10.1093/molbev/msw054>
- Larsen, J. (1994). Unarmoured dinoflagellates from Australian waters I. The genus *Gymnodinium* (Gymnodiniales, Dinophyceae). *Phycologia*, *33*(1), 24–33. <https://doi.org/10.2216/0031-8884-33-1-24.1>
- Manno, C., Stowasser, G., Enderlein, P., Fielding, S., & Tarling, G. A. (2015). The contribution of zooplankton faecal pellets to deep-carbon transport in the Scotia Sea (Southern Ocean). *Biogeosciences*, *12*(6), 1955–1965. <https://doi.org/10.5194/bg-12-1955-2015>
- Menden-Deuer, S., & Lessard, E. J. (2000). Carbon to volume relationships for dinoflagellates, diatoms, and other protist plankton. *Limnology & Oceanography*, *45*(3), 569–579. <https://doi.org/10.4319/lo.2000.45.3.0569>
- Michaels, A. F., Silver, M. W., Gowing, M. M., & Knauer, G. A. (1990). Cryptic zooplankton “swimmers” in upper ocean sediment traps. *Deep-Sea Research, Part A: Oceanographic Research Papers*, *37*(8), 1285–1296. [https://doi.org/10.1016/0198-0149\(90\)90043-U](https://doi.org/10.1016/0198-0149(90)90043-U)
- Moestrup, Ø., Hakanen, P., Hansen, G., Daugbjerg, N., & Ellegaard, M. (2014). On *Levanderina fissa* gen. & comb. nov. (Dinophyceae) (syn. *Gymnodinium fissum*, *Gyrodinium instriatum*, *Gyr. uncatenum*), a dinoflagellate with a very unusual sulcus. *Phycologia*, *53*(3), 265–292. <https://doi.org/10.2216/13-254.1>
- Motoda, S. (1959). Devices of simple plankton apparatus. *Memoirs of the Faculty of Fisheries Hokkaido University*, *7*(1–2), 73–94. Retrieved from <http://hdl.handle.net/2115/21829>
- Nagai, S., Yamamoto, K., Hata, N., & Itakura, S. (2012). Study of DNA extraction methods for use in loop-mediated isothermal amplification detection of single resting cysts in the toxic dinoflagellates *Alexandrium tamarense* and *A. catenella*. *Marine Genomics*, *7*, 51–56. <https://doi.org/10.1016/j.margen.2012.03.002>
- Nakamura, Y., Yamazaki, Y., & Hiromi, J. (1992). Growth and grazing of a heterotrophic dinoflagellate, *Gyrodinium dominans*, feeding on a red tide flagellate, *Chattonella antiqua*. *Marine Ecology Progress Series*, *82*(3), 275–279. <https://doi.org/10.3354/meps082275>
- Oksanen, J., Blanchet, F. G., Kindt, R., Legendre, P., Minchin, P. R., O'hara, R., et al. (2019). Package ‘vegan’: Community ecology package, version, 2.5-4. Retrieved from <https://cran.r-hub.io/web/packages/vegan/vegan.pdf>
- Passow, U., & Carlson, C. A. (2012). The biological pump in a high CO₂ world. *Marine Ecology Progress Series*, *470*(2), 249–271. <https://doi.org/10.3354/meps09985>
- Pauli, N. C., Flintrop, C. M., Konrad, C., Pakhomov, E. A., Swoboda, S., Koch, F., et al. (2021). Krill and salp faecal pellets contribute equally to the carbon flux at the Antarctic Peninsula. *Nature Communications*, *12*(1), 1–12. <https://doi.org/10.1038/s41467-021-27436-9>
- Peng, X., Yu, K. Q., Deng, G. H., Jiang, Y. X., Wang, Y., Zhang, G. X., & Zhou, H. W. (2013). Comparison of direct boiling method with commercial kits for extracting fecal microbiome DNA by Illumina sequencing of 16S rRNA tags. *Journal of Microbiological Methods*, *95*(3), 455–462. <https://doi.org/10.1016/j.mimet.2013.07.015>
- Poulsen, L. K., & Iversen, M. H. (2008). Degradation of copepod fecal pellets: Key role of protozooplankton. *Marine Ecology Progress Series*, *367*, 1–13. <https://doi.org/10.3354/meps07611>
- Poulsen, L. K., Moldrup, M., Berge, T., & Hansen, P. J. (2011). Feeding on copepod fecal pellets: A new trophic role of dinoflagellates as detritivores. *Marine Ecology Progress Series*, *441*, 65–77. <https://doi.org/10.3354/meps09357>
- Rembauville, M., Blain, S., Armand, L., Quéguiner, B., & Salter, I. (2015). Export fluxes in a naturally iron-fertilized area of the Southern Ocean—Part 2: Importance of diatom resting spores and faecal pellets for export. *Biogeosciences*, *12*(11), 3171–3195. <https://doi.org/10.5194/bg-12-3171-2015>
- Saito, H., Ota, T., Suzuki, K., Nishioka, J., & Tsuda, A. (2006). Role of heterotrophic dinoflagellate *Gyrodinium* sp. in the fate of an iron induced diatom bloom. *Geophysical Research Letters*, *33*(9), L09602. <https://doi.org/10.1029/2005GL025366>
- Schloss, P. D., Westcott, S. L., Ryabin, T., Hall, J. R., Hartmann, M., Hollister, E. B., et al. (2009). Introducing mothur: Open-source, platform-independent, community-supported software for describing and comparing microbial communities [Software]. *Applied and Environmental Microbiology*, *75*(23), 7537–7541. <https://doi.org/10.1128/AEM.01541-09>
- Schourup-Kristensen, V., Sidorenko, D., Wolf-Gladrow, D. A., & Völker, C. (2014). A skill assessment of the biogeochemical model REcoM2 coupled to the Finite Element Sea Ice-Ocean Model (FESOM 1.3). *Geoscientific Model Development*, *7*(6), 2769–2802. <https://doi.org/10.5194/gmd-7-2769-2014>
- Seuront, L., Leterme, S. C., Seymour, J. R., Mitchell, J. G., Ashcroft, D., Noble, W., et al. (2010). Role of microbial and phytoplanktonic communities in the control of seawater viscosity off East Antarctica (30–80° E). *Deep-Sea Research Part II Topical Studies in Oceanography*, *57*(9–10), 877–886. <https://doi.org/10.1016/j.dsr2.2008.09.018>
- Stamieszkin, K., Steinberg, D. K., & Maas, A. E. (2021). Fecal pellet production by mesozooplankton in the subarctic Northeast Pacific Ocean. *Limnology & Oceanography*, *66*(7), 2585–2597. <https://doi.org/10.1002/lno.11774>
- Steinberg, D. K., & Landry, M. R. (2017). Zooplankton and the ocean carbon cycle. *Annual Review of Marine Science*, *9*(1), 413–444. <https://doi.org/10.1146/annurev-marine-010814-015924>
- Svensen, C., Riser, C. W., Reigstad, M., & Seuthe, L. (2012). Degradation of copepod faecal pellets in the upper layer: Role of microbial community and *Calanus finmarchicus*. *Marine Ecology Progress Series*, *462*, 39–49. <https://doi.org/10.3354/meps09808>
- Taguchi, S., & Saino, T. (1998). Net zooplankton and the biological pump off Sanriku, Japan. *Journal of Oceanography*, *54*(5), 573–582. <https://doi.org/10.1007/BF02742459>
- Takano, Y., & Horiguchi, T. (2004). Surface ultrastructure and molecular phylogenetics of four unarmored heterotrophic dinoflagellates, including the type species of the genus *Gyrodinium* (Dinophyceae). *Phycological Research*, *52*(2), 107–116. <https://doi.org/10.1111/j.1440-1835.2004.tb00319.x>

- Turner, J. T. (2002). Zooplankton fecal pellets, marine snow and sinking phytoplankton blooms. *Aquatic Microbial Ecology*, 27(1), 57–102. <https://doi.org/10.3354/ame027057>
- Turner, J. T. (2015). Zooplankton fecal pellets, marine snow, phytodetritus and the ocean's biological pump. *Progress in Oceanography*, 130, 205–248. <https://doi.org/10.1016/j.pocean.2014.08.005>
- Villanueva, R. A. M., & Chen, Z. J. (2019). ggplot2: Elegant graphics for data analysis (2nd ed.). *Measurement: Interdisciplinary Research and Perspectives*, 17(3), 160–167. <https://doi.org/10.1080/15366367.2019.1565254>
- Wang, Y., Tian, R. M., Gao, Z. M., Bougouffa, S., & Qian, P. Y. (2014). Optimal eukaryotic 18S and universal 16S/18S ribosomal RNA primers and their application in a study of symbiosis. *PLoS One*, 9(3), e90053. <https://doi.org/10.1371/journal.pone.0090053>
- Wilson, S. E., Steinberg, D. K., & Buesseler, K. O. (2008). Changes in fecal pellet characteristics with depth as indicators of zooplankton repackaging of particles in the mesopelagic zone of the subtropical and subarctic North Pacific Ocean. *Deep-Sea Research Part II Topical Studies in Oceanography*, 55(14–15), 1636–1647. <https://doi.org/10.1016/j.dsr2.2008.04.019>
- Ye, J., Coulouris, G., Zaretskaya, I., Cutcutache, I., Rozen, S., & Madden, T. L. (2012). Primer-BLAST: A tool to design target-specific primers for polymerase chain reaction. *BMC Bioinformatics*, 13(134), 134. <https://doi.org/10.1186/1471-2105-13-134>
- Yokoi, N., Abe, Y., Kitamura, M., Honda, M. C., & Yamaguchi, A. (2018). Comparisons between POC and zooplankton swimmer flux from sediment traps in the subarctic and subtropical North Pacific. *Deep-Sea Research Part I Oceanographic Research Papers*, 133, 19–26. <https://doi.org/10.1016/j.dsr.2018.01.003>
- Yoon, W., Kim, S., & Han, K. (2001). Morphology and sinking velocities of fecal pellets of copepod, molluscan, euphausiid, and salp taxa in the northeastern tropical Atlantic. *Marine Biology*, 139(5), 923–928. <https://doi.org/10.1007/s002270100630>
- Zhao, S., Guo, Y., Sheng, Q., & Shyr, Y. (2014). Heatmap3: An improved heatmap package with more powerful and convenient features. *BMC Bioinformatics*, 15(S10), P16. <https://doi.org/10.1186/1471-2105-15-S10-P16>